ACS APPLIED MATERIALS & INTERFACES

Research Article

www.acsami.org

Electrospun Polystyrene Nanofiber Membrane with Superhydrophobicity and Superoleophilicity for Selective Separation of Water and Low Viscous Oil

Min Wook Lee,[†,§] Seongpil An,[†,§] Sanjay S. Latthe,[†] Changmin Lee,[†] Seungkwan Hong,[‡] and Sam S. Yoon*[,†]

[†]School of Mechanical Engineering and [‡]School of Civil, Environmental, and Architectural Engineering, Korea University, Seoul 136-713, Korea

Supporting Information

ABSTRACT: The ability to prepare solid surfaces with well-controlled superhydrophobic and superoleophilic properties is of paramount importance to water−oil separation technology. Herein, we successfully prepared superhydrophobic-superoleophilic membranes by single-step deposition of polystyrene (PS) nanofibers onto a stainless steel mesh via electrospinning. The contact angles of diesel and water on the prepared PS nanofiber membrane were 0° and 155° ± 3°, respectively. Applications of the PS nanofiber membrane toward separating liquids with low surface tension, such as oil, from water were investigated in detail. Gasoline, diesel, and mineral oil were tested as representative low-viscosity oils. The PS nanofiber membranes efficiently separated several liters of oil from water in a single step, of only a few minutes' duration. The superhydrophobic PS nanofiber membrane selectively absorbs oil, and is highly efficient at oil−water separation, making it a very promising material for oil spill remediation.

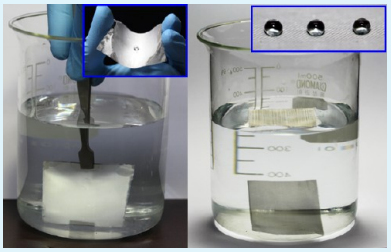

KEYWORDS: *PS nanofibers, electrospinning, membrane, superhydrophobic, superoleophilic, oil−water separation*

1. INTRODUCTION

Oil contamination is a major source of water pollution, especially in areas that have experienced industrial and urban expansion. Oil and fuel spills caused by industrial accidents or oil transport accidents are catastrophic for marine and aquatic ecosystems. Catastrophic oil spills, such as that in the Gulf of Mexico, remind us of the necessity for prompt action to develop an environmentally friendly, cost-effective, and large-scale technology to minimize environmental damages caused by such oil-spill disasters.[1] Conventional oil−water separation methods such as coagulation−flocculation, skimming, centrifugation, and gravity separation exhibit shortcomings, including low separation efficiency, high operation costs, cumbersome equipment, and the generation of secondary pollutants.[2] Several absorbent materials, including zeolites,[3] activated carbon, hair,[4] organoclays,[5] gelators derived from sugar[6] or straw,[7] carbon nanotube sponges,[8] wool fibers,[9] and others[10] have been considered as potential oil−water separators. Novel technologies to assist in the cleanup of these disasters have focused on materials that interact with oil and water in different ways. The main properties of an ideal sorbent material for an oil spill cleanup would include high hydrophobicity, high uptake capacity and rate, buoyancy, retention over time, durability in aqueous media, reusability or biodegradability, and recoverability of the absorbed oil.[11]

Biomimetics are materials that mimic nature. In the case of wettable and nonwettable surfaces, nature provides many models for their development. Several plants and animals exhibit superhydrophobic surfaces having water contact angles greater than 150° and sliding angles less than 10°; these have inspired many exciting models of functional bioinspired surfaces.[12,13] One of the most well-known natural superhydrophobic surfaces is that of the leaf of lotus, that is, *Nelumbo nucifera*.[14] Numerous studies attribute the superhydrophobic behavior of the lotus leaf surface to a combination of surface chemistry and surface roughness on multiple scales. However, a liquid with low surface tension, such as hexadecane (γ_{lv} = 27.5 mN/m), spreads rapidly across the lotus leaf, resulting in a contact angle of ∼0°.[15] The surface tension of water is commonly much larger than that of oil. Therefore, if the surface tension of a solid surface lies between those of water and oil, it might show both hydrophobicity and oleophilicity.[16] Superhydrophobic surfaces generally show superoleophilicity because of their high roughness[17] and because these surfaces generally comprise materials whose surface energy is similar to that of oil, thus quite different from that of water. The surface tension difference between water (72.8 mN m^{-1}) and oil (less than 30 mN m^{-1}) helps illustrate why superhydrophobic surfaces are usually oleophilic or superoleophilic.[18] Wettability, which is one of the most important properties of solid surfaces, can be controlled by manipulating both the surface chemistry and the surface geometrical structure of a material.[19−21] The wetting of

Received: June 25, 2013
Accepted: October 2, 2013
Published: October 3, 2013

rough surfaces has been theoretically explained by the Wenzel model[22] and the Cassie–Baxter model.[23] Solid surfaces with such unusual wettability, possessing not only superhydrophobicity but also superoleophilicity, have attracted great interest because of their potential in a wide range of practical applications.[24] Materials with both hydrophobic and oleophilic properties are preferred for oil collection because they allow proper oil disposal and minimize secondary pollution. To date, superhydrophobic and superoleophilic meshes,[25] films,[26] and membranes[27] have been used as filters that allow oil to penetrate through them but water to remain on their surfaces. Feng et al. prepared superhydrophobic, superoleophilic, stainless steel mesh substrates by spraying polytetrafluoroethylene onto the mesh substrates for their use in separating oil from water.[16] Zhang et al. fabricated a superhydrophobic and superoleophilic membrane by immersing a porous polyurethane (PU) film into a polystyrene (PS) colloidal solution.[26] Xue et al. reported a novel hydrogel-coated mesh for oil/water separation.[28] Zhu et al. presented a simple method for removing and collecting oils and organic solvents from surfaces of water based on superhydrophobic and superoleophilic sponges that were fabricated by solution immersion.[29] Lee et al. synthesized vertically aligned, multiwalled carbon nanotubes on a stainless steel mesh for separation of oil and water.[2] Both superhydrophobicity and superoleophilicity were obtained from its low surface energy and dual-scale structure composed of needle-like nanotubes on a microscale mesh. Recently, Zhang et al.[30] successfully used a simple chemical vapor deposition (CVD) method to grow silicone nanofilaments on a commercial polyester textile, which modified the textile to be superhydrophobic and superoleophilic. Despite all of the aforementioned studies, the large-scale fabrication of such functional membranes and their practical applications is limited by expensive and complex fabrication procedures, lack of ability to withstand harsh practical conditions, low stability and flexibility, as well as their poor selectivity and recyclability.

A number of hybrid materials can be electrospun into fibers with diameters ranging from a few nanometers to micrometers, depending on the viscosity and concentration of the source solution, the molecular weight of the precursor used, and the applied voltage.[31] Electrospun membranes consisting of a continuous, nonwoven web of nanofibers usually have a high surface area-to-volume ratio, complex pore structure, and other unique physical and mechanical properties that make them ideal materials for filtration applications.[32] PS membranes fabricated by electrospinning can have a water contact angle as high as 160°.[33] Recently, Shang et al.[34] fabricated superhydrophobic-superoleophilic nanofibrous membranes by in situ polymerization of electrospun cellulose acetate (CA) nanofibers, coated with a layer of SiO_2 nanoparticles that were functionalized with fluorinated polybenzoxazine. The fabrication of submicrometer-sized fiber mats by electrospinning offers opportunities to improve oil–water separations.[35] Fiber materials with low surface energies confer oleophilic properties upon the membranes. The enhanced hydrophobicity and oleophilicity of these surfaces is useful in oil–water separations.[36]

In the present work, we report a simple, versatile, low-cost, one-step method for the preparation of superhydrophobic and superoleophilic PS nanofiber membranes on a stainless steel mesh by electrospinning and report the application of the PS nanofiber membranes for the separation of low-viscosity oil from water. Our prepared PS nanofiber membranes cannot be used for the separation of high-viscosity oils from water because of the small size of their pores that are made of randomly deposited electrospun PS nanofibers. The flow of high-viscosity oil through these pores would be very slow, and oil–water separation could last several months, which would be impractical.

2. EXPERIMENTAL SECTION

2.1. Materials. Pellet type white-colored PS ($(C_8H_8)_n$, melting/boiling point 212 °C, refractive index 1.5916, M_w = 192,000 kg/kmol) was purchased from Sigma Aldrich (Missouri, U.S.A.), and dimethylformamide (DMF) and nitric acid (HNO_3) were purchased from Duksan Chemical (Ansan, South Korea). The base substrate was a stainless steel mesh with pore size of ~30 μm, purchased from HanKook Metal (Seoul, South Korea). Gasoline, diesel, and mineral oil (SK energy, Seoul, South Korea) were tested, as representative low-viscosity oils.[37] The thermo-physical properties of these oils are listed in Table 1. Double distilled, deionized water (Human Science, HIQI) was used in all experimental steps (e.g., rinsing and dilution) to avoid any impurities that would affect the final results. The filter holder and container were commercially obtained and modified in our laboratory.

Table 1. Thermo-Physical Properties of Gasoline, Diesel, and Mineral Oil

	viscosity [cP]	density [g/cm^3]	surface tension [N/m]
diesel	3.0	0.83	0.03
gasoline	0.5	0.75	0.02
mineral oil	10.3	0.84	0.02

2.2. Synthesis of PS Nanofiber Membrane. A PS nanofiber membrane was prepared on a stainless steel mesh by electrospinning at room temperature, as follows. PS was dissolved in dimethylformamide (DMF) to a concentration of 20 wt %. A few drops of nitric acid were added to the PS solution to render it electrically conductive (K = 35 μS/cm) without changing its viscosity and surface tension. This PS solution was then stirred continuously for 24 h prior to electrospinning. During electrospinning, the flow rate of the precursor solution was set at 180 μL/h via syringe pump to yield a stable Taylor cone. The needle used had an inner diameter of 0.25 mm. A voltage-supply wire was attached to the charging needle, and the substrate was grounded. A voltage of 5.0 kV was applied to the needle to yield nanofibers. The stainless steel mesh was cleaned by absolute ethanol and acetone rinses before the electrospinning deposition. The deposition time, t_{dep}, was kept constant at 5 min.

2.3. Characterization of PS Nanofiber Membrane. The surface microstructure and fiber diameters of the PS nanofiber membrane were characterized by high-resolution scanning electron microscopy (S-5000, Hitachi at 15 kV). The fiber diameters were calculated from the SEM images. Supporting Information, Figure S1 shows a typical nanofiber size distribution of the membrane, with an average fiber diameter of 317 nm. These fibers were collected from the center of the membrane. However, we also collected fibers near the periphery of the membrane, and we found that their morphology was quite similar to that of the central fibers. Thus, we are confident that the Gaussian distribution in Supporting Information, Figure S1 represents the typical fiber size distribution of the membrane.

The wettability of the PS nanofiber membranes was determined by static water-contact-angle measurements in open air. A goniometer was used to measure and record the static contact angle of DI water on the PS nanofiber membranes. The contact angle was measured after the drop had rested for 5 s on the PS nanofiber membrane. The DI water was supplied to a stainless-steel nozzle (EFD, inner and outer diameters of 250 and 520 μm, respectively) by a syringe pump (KDS Legato 100) at a flow rate of 180 μL/h. All measurements and experiments were performed at ambient conditions and room temperature. The average static water contact angle was obtained from measurements taken at five different positions on the same

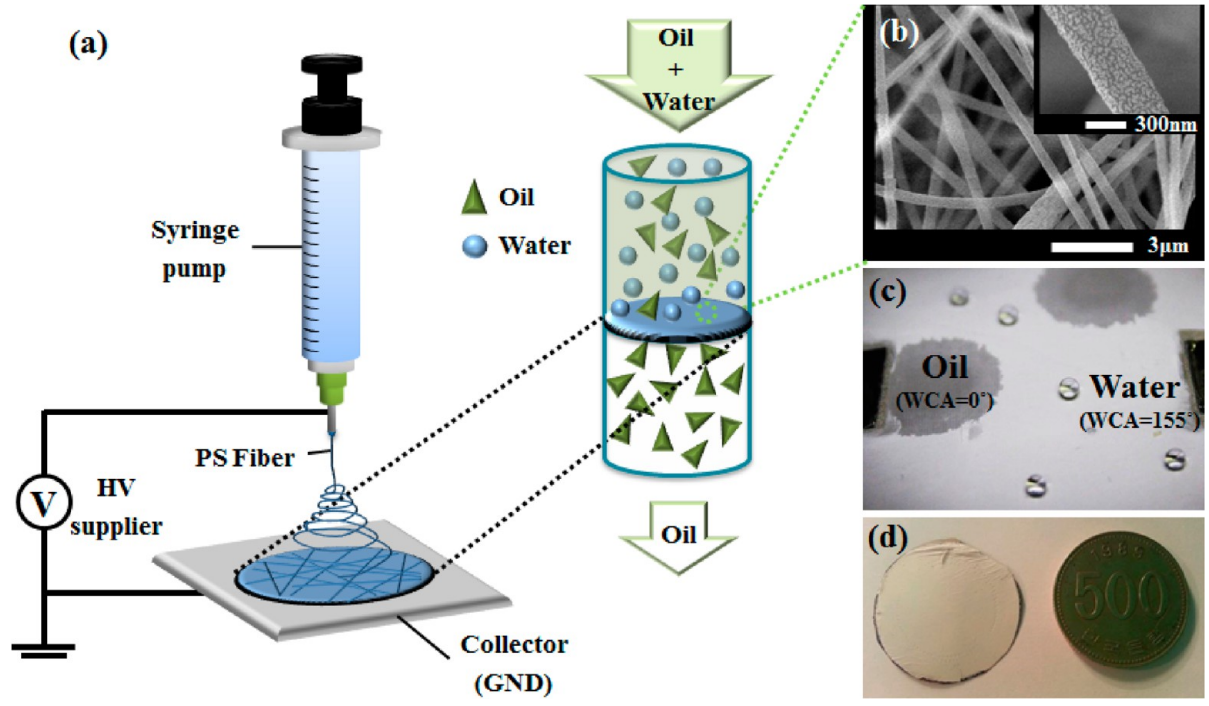

Figure 1. (a) Schematic showing the electrospun membrane fabrication process. (b) SEM images with high and low magnifications. (c) A photograph showing superoleophilic and superhydrophobic PS nanofiber membrane. (d) The real scale as-prepared PS nanofiber membrane attached to the stainless mesh, whose size is compared with a coin.

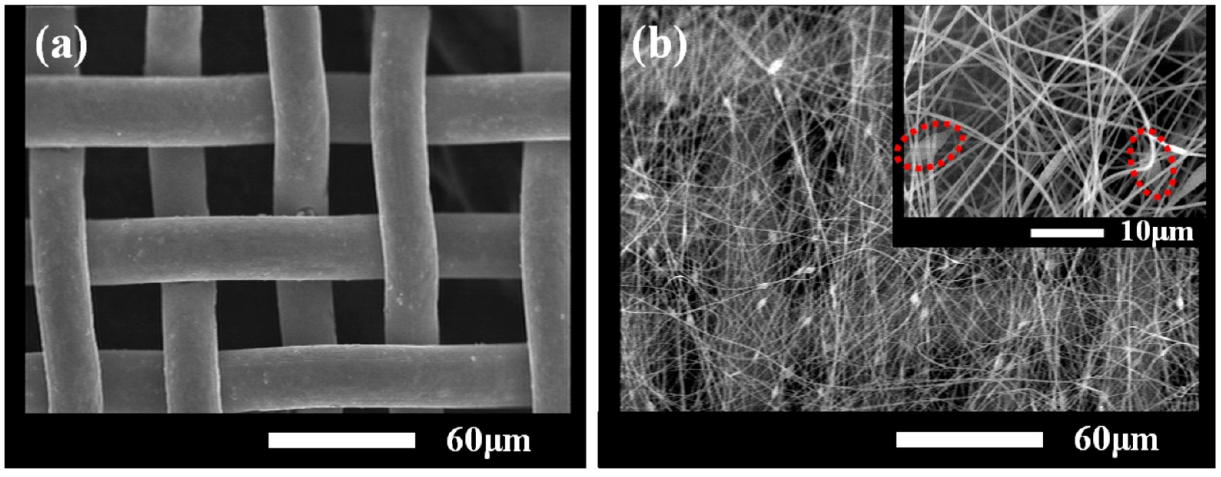

Figure 2. (a) SEM image of the stainless steel mesh with an average square-shaped pore size of approximately 30 μm. (b) A SEM image of the PS nanofiber membrane synthesized on the stainless steel mesh (with red dotted circles showing elliptical bead-on-string structure).

sample. The specific surface area, pore volume, and pore diameter of the membranes were determined by performing Brunauer–Emmett–Teller (BET) analysis on the results of nitrogen multilayer adsorption (ASAP 2010 Analyzer BET)

2.4. Superhydrophobicity and Superoleophilicity. The superoleophilicity of the membranes was tested by locating the membrane between two beakers. Silicone glue was used to seal the two beakers together, and we confirmed no leakage. Diesel oil (100 mL) was initially located in the bottom beaker. Inverting the beakers caused oil to pour onto the membrane. The superoleophilicity of the membrane allowed oil to filter via gravity through the membrane from the top beaker to the bottom beaker. The area of the membrane was 3.1 cm^2 and the beaker size was 250 mL per beaker. The membrane maintained superhydrophobicity up to a few kPa, estimated using the hydrostatic pressure, $\Delta P = \rho gh$, from the vertical installation of the membrane flow driven by gravity.

2.5. Oil–Water Separation Setup. The superhydrophobicity of the membrane was first tested by placing it between two beakers, where the bottom beaker contains a mixture of water and oil, and then inverting the beakers so that the water/oil mixture is in the top beaker. However, using this setup, oil cannot flow from one beaker to the other because the higher density of water causes it to form a barrier layer between the oil and the membrane. For this reason, an alternative test setup was devised as follows. The diesel-water mixture was instead contained in a syringe that was set horizontally, and its plunger was pressed at a constant rate by a syringe pump. The flow rate of the syringe pump was varied from 1 to 10 mL/min. The faster the piston movement, the higher the flow rate. This pressure-driven flow pushes both diesel and water to the membrane simultaneously. Oil flows through because of the superoleophilicity of the membrane, and water remains behind because of the superhydrophobicity of the membrane. In this way, the extent of diesel separation can be characterized from the varying flux of the diesel-water mixture. The operating pressure

imposed on the membrane was estimated to be about 800 kPa from the given piston force of 133 N over the piston area of 1.67×10^{-4} m^2.

3. RESULTS AND DISCUSSION

3.1. Surface Morphology of the PS Nanofiber Membranes. Electrospinning typically yields fibers that exhibit one of three typical morphologies: beads, beads-on-string, and fibers. These different structures can be obtained by adjusting the process parameters, that include the precursor's thermophysical properties as well as the operating conditions of electrospinning.[38] We attempted to avoid a bead-like structure to the greatest extent possible, because the beads-on-string structure causes nonuniformity in the structure of the membrane. The beads were prevented by adding HNO_3, which increased the electrical conductivity of the PS solution, rendering maximal the effect of electrical forces, and minimal the effect of surface tension.[38] Figure 1a shows a schematic of the electrospinning deposition, Figure 1b shows SEM images of the PS nanofiber membrane at high and low magnification, Figure 1c shows a snapshot showing oil and water droplets on the PS nanofiber membrane, and Figure 1d shows the real scale as-prepared PS nanofiber membrane attached to the stainless mesh.

The PS nanofibers electrospun on the stainless steel mesh are shown in Figure 2. In particular, Figure 2a shows a SEM image of the stainless steel mesh, which exhibits square-shaped pores of average size 30 μm. After electrospinning, a dense layer of randomly grown PS nanofibers was clearly observed on the surface of the stainless steel mesh (Figure 2b), decreasing the size of the pores and exhibiting randomly oriented, three-dimensional, nonwoven, and porous structures. The high porosity was due to the entanglement of the nanofibers, where all the pores (or the void spaces) were fully interconnected. BET analysis indicated that the porous membrane had a pore volume of 0.8613 cm^3/g, and a specific surface area of 81.51 m^2/g. These specifications may be compared with those of Lin et al.,[39] whose PS nanofibers were also spun from a 20 wt % solution of PS in DMF, and had a fiber diameter of 1800 nm, a pore volume of 0.067 cm^3/g, and a specific surface area of 12.23 m^2/g. Our fibers are 6 times smaller in diameter, 13 times larger in pore volume, and 6.7 times greater in specific surface area. This comparison indicates that the smaller the fiber diameter, the greater the pore volume and the specific surface area, which is expected. The greater pore volume would permit the larger flow rate. Moreover, the greater surface area would permit more interfacial activities.

The structure of the PS nanofiber membrane was observed in detail via SEM images at different magnifications, as shown in Figure 2(b) inset. As shown in Figures 1(b) and 2(b), the PS nanofiber membranes exhibited elliptical bead-on-string structures, comprising thin fibers (average diameter of 317 nm) with numerous nano- to microsized elliptical beads (average diameter of 2.45 μm) along the fiber axis. The beads are indicated by red dotted circles in the images. These structures are typical for the electrospinning of solutions with low viscosity or low polymer concentration during the electrospinning process.[40] However, the individual PS nanofibers had a nanotextured surface; see the inset of Figure 1(b). The hierarchical surface structure of the PS nanofibers enhanced the superhydrophobicity of the membrane, by forming a larger "air cushion" along the contacts between the droplets and the membrane.[41]

It should be noted that we have used the standard and routine electrospinning process. It may be understood that the fiber diameter seems a bit bulky or broad in some areas. These features are known as "beads". The size and appearance of the beads can be controlled by controlling the electrical conductivity of the solvent.[38] We added nitric acid to enhance the electrical conductivity, toward achieving uniform production of the nanofibers without beads. In the current work, the moderate electrical conductivity of our PS solution did not allow the beads to be completely eliminated. However, to the best of our knowledge, this existence of the beads is not of major concern regarding the membrane performance.

It is also worthwhile to note that both superhydrophobicity and superoleophilicity would decrease if the porous structure of the PS nanofibers was eliminated. To confirm the influence of the porous structure, we dip-coated a glass substrate with the PS solution to produce a nonporous homogeneous PS film. We found that the water contact angle reduced while the diesel contact angle increased, as shown in Supporting Information, Figure S2. In other words, both the superhydrophobicity and superoleophilicity were indeed reduced in the absence of the porous nanofiber structure.

3.2. Wetting Behavior of the PS Nanofiber Membranes. The wetting behavior of the PS nanofiber membrane was studied in detail. The uncoated stainless steel mesh was readily wetted by both water and oil, while the nanofiber membrane exhibited different wetting behavior toward water versus toward oil. Figure 1c is an optical image of oil and water droplets on the PS nanofiber membrane, and Figure 1d displays a photograph of the as-prepared PS nanofiber membrane. In Figure 1c, a water droplet sits on the membrane surface at a water contact angle of $155 \pm 3°$. Because of the superhydrophobicity of the PS nanofiber membrane the water droplets rolled off freely in any direction upon slight tilting of the surface (sliding angle $\sim 5 \pm 2°$), indicating a Cassie–Baxter nonwetting state. Such a low sliding angle revealed that the water could not penetrate into the surface structures and instead rested on the asperities of the surface with minimum liquid solid adhesion. This roll-off behavior implies that the PS nanofiber membrane was coated uniformly under atmospheric conditions. The wetting behavior of a diesel droplet is also shown in Figure 1c. The diesel droplet ($\sim$ 8 μL) spread out immediately on the membrane, with a contact angle of 0°, showing the strong superoleophilicity of the membrane. The diesel droplets wetted the membrane in only 0.5 s, which is at least 10 times faster than on the original stainless steel mesh, where the droplets remained intact for more than 5 s. These observations confirm that the as-prepared PS nanofiber membranes are highly superoleophilic and superhydrophobic.

The unique dual wettability of the PS nanofiber membrane is a result of its surface structure and fiber structure. The large content of air in the membrane system makes the surface more hydrophobic, leading to the large water contact angle.[25] Meanwhile, the hierarchical surface features promote the superoleophilic behavior, where capillary forces cause the oil droplets to fully wet the rough PS nanofiber surface, after which they penetrate the steel mesh via gravity.[42] As the oil wets the PS membrane, air in the gaps and voids of the PS nanofibers is replaced by the oil, on which a water droplet exhibits a reduced contact angle of 105°. The distinct boundary between the water droplet and the PS nanofibers remains intact despite the reduction in water contact angle. The surface tension of oil is

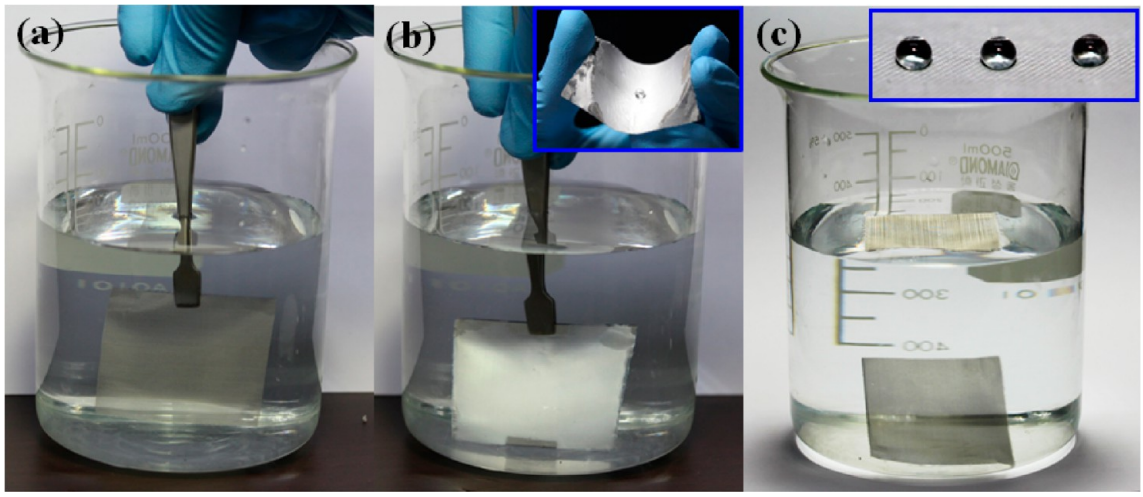

Figure 3. (a) Complete wetting of uncoated stainless steel mesh in water. (b) After immersing the PS nanofiber membrane in water, a plastron layer is formed (inset displays the spherical water droplet on bent membrane surface). (c) The uncoated stainless steel mesh sinks in the water and rests at the bottom of the beaker, whereas, the PS nanofiber membrane floats freely on the water surface confirming extreme water repellency. The inset displays the spherical water drops resting on the PS nanofiber membrane.

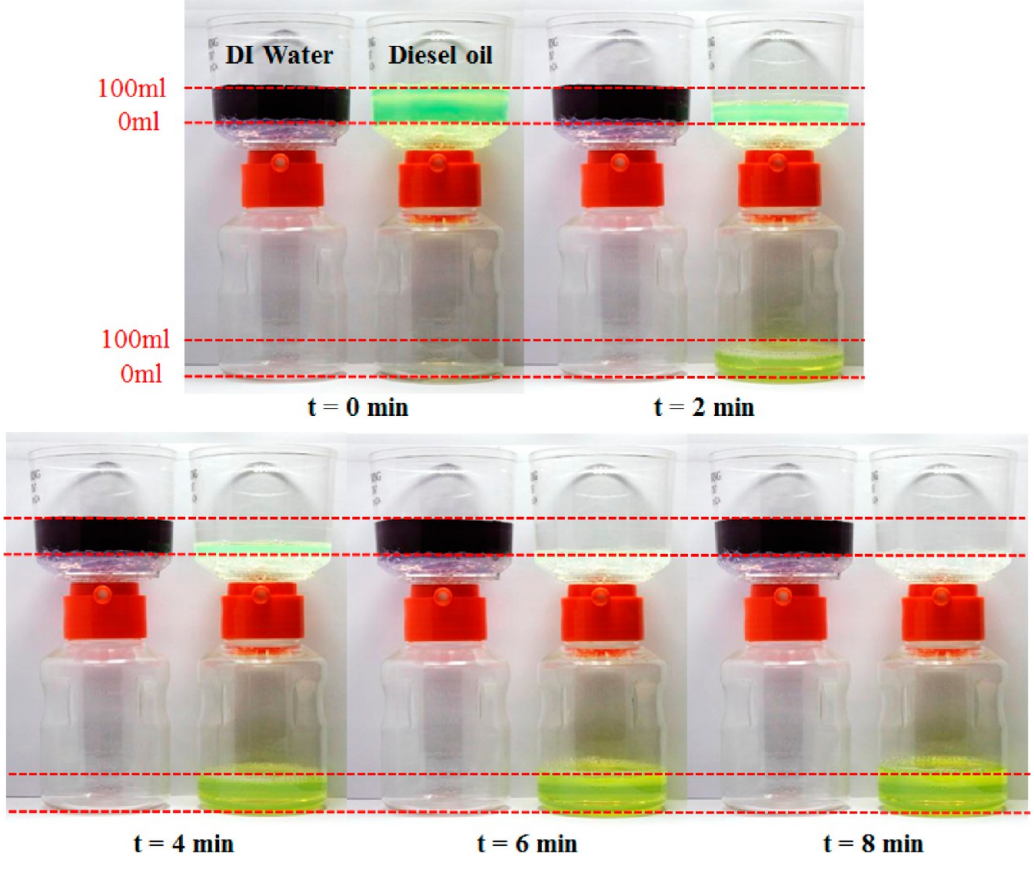

Figure 4. Experiments showing superhydrophobicity and superoelophilicity of the membrane. The left setup shows the nonpermeable nature of the membrane for DI water (dyed with black ink). The right setup shows the permeable nature of the membrane for diesel (lemon color).

much lower than that of water, which also contributed to the difference in the ability of each liquid to wet the membrane.

The differential wettability of the coated textile toward water and oil indicates promising applications for separating oil and water. However, it must be noted that the use of our membrane is currently limited to a pressure range of a few kPa. This pressure was estimated by using the hydrostatic pressure, $\Delta P = \rho gh$, from the gravity-driven vertical flow rate across the membrane. We have tested the membrane's durability up to approximately 10 kPa, that is, up to a water height of h = 1 m, which corresponds to a ΔP of about 10 kPa where $\Delta P = \rho gh = (1000\ \text{kg/m}^3)(9.8\ \text{m/s}^2)(1\ \text{m})$. Thus, the membrane was able to withstand 10 kPa of pressure. However, at pressures greater than 10 kPa, the membrane did not maintain its superhydrophobicity and became permeable to water.

dx.doi.org/10.1021/am404156k | ACS Appl. Mater. Interfaces 2013, 5, 10597−10604

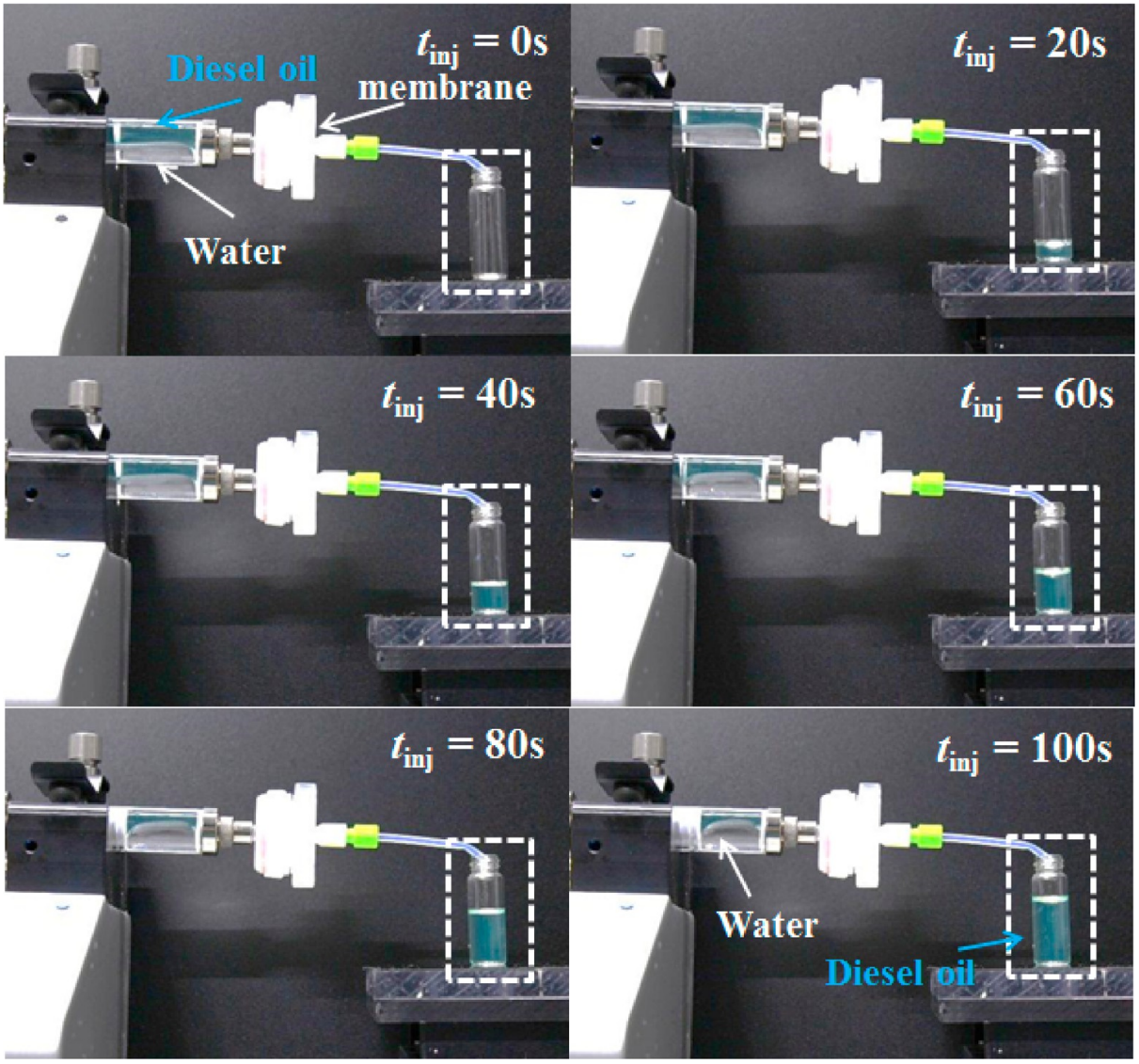

Figure 5. Setup for the oil–water separation by a syringe pump using DI water (transparent on bottom) and diesel oil (light blue on top). The operating conditions for the syringe pump were Q = 2 mL/min of both water and diesel, t_{inj} = 100 s, and A_{mem} = 4.9 cm^2. The volume of water and diesel was 3 and 5 mL, respectively.

Figure 3 confirms the existence of a plastron layer, or air cushion, between the PS nanofiber membrane and water, as well as the high water repellency of the membrane. Figure 3a shows an uncoated stainless steel mesh in water; the mesh is completely wetted by the water. Figure 3b shows the plastron layer on the PS nanofiber membrane after immersion in water. The air cushion between the membrane and water is visible as a shiny silvery layer because of the total internal reflection of light. The air cushion contributes to the superhydrophobicity of the membrane because most of the area beneath the water is a liquid–air interface, rather than a liquid–solid interface. This observation implies weak interaction between water and the membrane. When the membrane was immersed into water, it strongly repelled water and remained dry after it was removed from the water. The inset of Figure 3b shows the spherical water droplet on the flexible membrane. The adhesion is strong enough to hold the PS membrane even after bending the membrane multiple times. This is best described in Figure 3b, where the membrane does not detach from the substrate even after repeated bending. The extreme water repellency of the membrane is confirmed in Figure 3c, which shows that the uncoated stainless steel mesh immediately sinks in the water and rests at the bottom of the beaker, whereas the PS nanofiber membrane floats freely on the water surface. The insets of Figure 3c display the spherical water drops resting on the PS nanofiber membrane.

Variation in contact angle is critical to applications that utilize superhydrophobicity or superhydrophilicity. To characterize the durability of our membrane, that is, to analyze the deterioration of the hydrophobic state, we evaluated the variation in contact angle with time.[43] Deionized water was used as the test liquid. The water droplets retained a quasi-spherical shape while resting for 30 min on the PS nanofiber membrane surface, and rolled off readily upon slight tilting. This simple test indicates the durability of the membrane's superhydrophobicity even after lengthy exposure to water. The flexibility of the membrane is demonstrated by its ability to be bent and returned to its original shape at least a hundred times without cracks.

3.3. Superhydrophobicity and Superoleophilicity. The superhydrophobicity and superoleophilicity of the membrane were tested using a simple setup, as shown in Figure 4. The membrane used herein was fabricated with the nanofiber deposition time of 5 min, as noted in Section 2.2. The experimental setup shown in Figure 4 consists of two beakers with the membrane sealed between them. The water was dyed black using a water-based ink, and the diesel was used as-received. Both water and diesel were put inside the top beaker separately in the left and right setup, respectively. The diesel penetrates through the membrane and is collected into the beaker beneath the membrane. All 100 mL of diesel completely permeated through the membrane within 8 min, driven only by gravity and the capillary flow because of the strong oleophilicity of the PS nanofibers. Almost all of the diesel was collected in the beaker.

Meanwhile, water was retained above the membrane because of the superhydrophobicity and low water adhesion of the membrane. Water did not leak through the filter membrane even after 24 h. This lack of water leakage demonstrates the excellent superhydrophobic characteristics of the PS nanofiber membrane. The membrane had no visible change after its immersion in water.

3.4. Oil–Water Separation. To test the membrane's performance under more severe conditions compared to the simple gravity-driven flow shown in Figure 4, we used a syringe pump that yielded a pressure-driven flow for both oil and water. In this case, the flow rate (or flux) of the syringe pump was fixed at 2 mL/min and did not change with time. In general, the pressure and flow rate can be related by the simple Poiseuille's law which accounts for the viscous effect over a constant size circular pipe.[44] However, in this case, a syringe pump is subject to sufficiently large force (i.e., > 133 N)[45] to drive a flow of any viscosity, but the flow rate is controlled by the piston's maneuvering speed. Thus, the flow rate and pressure cannot be linearly related by the simple Poiseuille's law for a syringe pump.

Various types of oil were tested, including diesel, gasoline, and mineral oil; the results are shown in Figure 5, Supporting Information, Figures S3, S4, respectively. The membrane was installed in such a manner as to allow both diesel and water to pass through the membrane simultaneously, as shown in Figure 5. The syringe piston was stopped on purpose at about t_{inj} = 100 s when the membrane started to leak water after filtering enough oil from the syringe cylinder to the collecting glass on right. This is natural because, after enough filtering of oil, there remains largely water and little oil in the cylinder and thus the only option is to permeate water through the membrane. This phenomenon was evidenced in Supporting Information, Figure S5.

Despite its superhydrophobicity, the membrane would be expected to allow the permeation of water at a sufficiently high pressure, in the absence of diesel. Figure 5 shows the experimental setup for the separation in this case, where a horizontally installed syringe pump that included diesel on top and water at bottom. Both diesel and water were in contact with the vertically installed membrane, which is noted as "membrane" in the snapshot corresponding to t_{inj} = 0 s in Figure 5. The pump flow rate was set to Q = 2 mL/min and the cross-sectional area of the syringe was A_{mem} = 4.9 cm^2. When both liquids were in contact with the membrane, its superoleophilicity caused the oil to be permeated through the membrane. This resulted in the accumulation of diesel inside the container, which is indicated inside the dashed box in Figure 5. The accumulation of diesel inside the container, without any accumulation of water continued up to t_{inj} = 100 s. On the other hand, the superhydrophobicity of the membrane caused it to deform because of the pressure of the water, which could not permeate the membrane; see the snapshot at $t_{inj} \geq 20$ s. From Figure 5, the membrane achieves nearly 100% separation efficiency of water and oil as long as the injection pressure is low; the flow rate of Q = 2 mL/min was also low. The swelling was caused by the accumulation of water that was not able to permeate through the membrane because of its superhydrophobicity. The deformation continued until the syringe was mostly occupied by water while most of diesel had permeated through the membrane. Eventually, the diesel was completely separated or removed from the syringe. The oil absorption capacity of the PS nanofiber membrane can be attributed to the highly porous structure of PS nanofibers.[46] The mechanisms by which oil becomes incorporated into the PS nanofibers are adsorption, capillary action, or a combination of these. At the initial stage of oil sorption onto the PS nanofiber membrane, oleophilic interaction and van der Waals forces may play an important role at the interface between the oil and the membrane.[47] In other superoleophilic materials, it is believed that the diesel is adsorbed by physical trapping on the fiber surface, thus filling the voids between nanofibers. As a result, the oil diffuses into the porous interior of the fibers via capillary action through the fiber cuticle or ends.[48] We carefully note that the membrane can only be used once because PS is vulnerable to aromatic hydrocarbons, such as benzene, toluene, xylene, and ethylbenzene.[49] Diesel comprises 75% saturated hydrocarbons and 25% aromatic hydrocarbons and thus diesel dissolves PS. We took a SEM image of the membrane after its 2-h exposure to diesel; see Supporting Information, Figure S6. The membrane was used as an oil–water separator and then was dried in an open air condition for 2 h. The PS fibers were completely dissolved in a manner in which their dissolved residues are attached to the stainless mesh, leaving a "centipede-like" mark. We also tested the separation capability of PS membranes having different thicknesses. To vary the thickness, we varied the deposition time of the PS nanofibers from 3 to 20 min. Changing the thickness over this range did not affect the separation capability (not shown here).

4. CONCLUSIONS

We successfully prepared superhydrophobic-superoleophilic membranes by single-step deposition of PS nanofibers onto a stainless steel mesh by electrospinning. The fabrication technique was simple, and the materials used were inexpensive. The combination of low free energy PS nanofibers with the three-dimensional network structures of the membrane enhanced the nonwetting of water while keeping the intrinsic wetting of oil, resulting in superoleophilic and superhydrophobic membranes. These membranes easily separated diesel oil from water. The PS nanofiber membranes also exhibited excellent superhydrophobicity even after many cycles of the oil–water separation process. These membranes are highly efficient, making them a suitable and inexpensive method to remove many types of organic solvents or oils from water at large production scales.

■ ASSOCIATED CONTENT

Supporting Information

Additional information regarding nanofiber size distribution, the contact angle of water and diesel drops on PS-coated film, and the oil−water separation (i.e., gasoline and mineral-oil) are provided. This material is available free of charge via the Internet at http://pubs.acs.org.

■ AUTHOR INFORMATION

Corresponding Author

*E-mail: skyoon@korea.ac.kr.

Author Contributions

§Equal contribution.

Notes

The authors declare no competing financial interest.

■ ACKNOWLEDGMENTS

This work was supported by the National Research Foundation of Korea (2013R1A2A2A05005589) grant funded by the Korea government (MEST). This research was also supported by the Converging Research Center Program through the Ministry of Education, Science and Technology (2013K000186), the Center for Inorganic Photovoltaic Materials (No. 2012-0001169), and the Korea Research Council Industrial Science and Technology (B551179-08-03-00). This work was supported by the Global Frontier R&D Program (2013-073298) on Center for Hybrid Interface Materials (HIM) funded by the Ministry of Science, ICT & Future Planning.

■ REFERENCES

(1) Arbatan, T.; Fang, X.; Shen, W. *Chem. Eng. J.* **2011**, *166*, 787−791.
(2) Lee, C.; Baik, S. *Carbon* **2010**, *48*, 2192−2197.
(3) Radetic, M. M.; Jocic, D. M.; Jovancic, P. M.; Petrovic, Z. L.; Thomas, H. F. *Environ. Sci. Technol.* **2003**, *37*, 1008−1012.
(4) Bayat, A.; Aghamiri, S. F.; Moheb, A.; Vakili-Nezhaad, G. R. *Chem. Eng. Technol.* **2005**, *28*, 1525−1528.
(5) Adebajo, M. O.; Frost, R. L.; Kloprogge, J. T.; Carmody, O.; Kokot, S. *J. Porous Mater.* **2003**, *10*, 159−170.
(6) Jadhav, S. R.; Vemula, P. K.; Kumar, R.; Raghavan, S. R.; John, G. *Angew. Chem., Int. Ed.* **2010**, *49*, 7695−7698.
(7) Choi, H. M.; Cloud, R. M. *Environ. Sci. Technol.* **1992**, *26*, 772−776.
(8) Lee, C. H.; Johnson, N.; Drelich, J.; Yap, Y. K. *Carbon* **2011**, *49*, 669−676.
(9) Annunciado, T. R.; Sydenstricker, T. H. D.; Amico, S. C. *Mar. Pollut. Bull.* **2005**, *50*, 1340−1346.
(10) Nadargi, D. Y.; Latthe, S. S.; Hirashima, H.; Rao, A. V. *Microporous Mesoporous Mater.* **2009**, *117*, 617−626.
(11) Jiang, G.; Hu, R.; Wang, X.; Xi, X.; Wang, R.; Wei, Z.; Li, X.; Tang, B. *J. Text. Inst.* **2013**, *104*, 790−797.
(12) Xia, F.; Jiang, L. *Adv. Mater.* **2008**, *20*, 2842−2858.
(13) Liu, M.; Wang, S.; Wei, Z.; Song, Y.; Jiang, L. *Adv. Mater.* **2009**, *21*, 665−669.
(14) Barthlott, W.; Neinhuis, C. *Planta* **1997**, *202*, 1−8.
(15) Tuteja, A.; Choi, W.; Ma, M.; Mabry, J. M.; Mazzella, S. A.; Rutledge, G. C.; McKinley, G. H.; Cohen, R. E. *Science* **2007**, *318*, 1618−1622.
(16) Feng, L.; Zhang, Z.; Mai, Z.; Ma, Y.; Liu, B.; Jiang, L.; Zhu, D. *Angew. Chem., Int. Ed.* **2004**, *43*, 2012−2014.
(17) Yao, X.; Song, Y.; Jiang, L. *Adv. Mater.* **2011**, *23*, 719−734.
(18) Cheng, Y.-T.; Rodak, D. E. *Appl. Phys. Lett.* **2005**, *86*, 144101−144103.
(19) Latthe, S. S.; Dhere, S. L.; Kappenstein, C.; Imai, H.; Ganesan, V.; Rao, A. V.; Wagh, P. B.; Gupta, S. C. *Appl. Surf. Sci.* **2010**, *256*, 3259−3264.
(20) Dhere, S. L.; Latthe, S. S.; Kappenstein, C.; Pajonk, G.; Ganesan, V.; Rao, A. V.; Wagh, P. B.; Gupta, S. C. *Appl. Surf. Sci.* **2010**, *256*, 3624−3629.
(21) Latthe, S. S.; Imai, H.; Ganesan, V.; Kappenstein, C.; Rao, A. V. *J. Sol-Gel Sci. Technol.* **2010**, *53*, 208−215.
(22) Wenzel, R. N. *Ind. Eng. Chem.* **1936**, *28*, 988−994.
(23) Cassie, A. *Discuss. Faraday Soc.* **1948**, *3*, 11−16.
(24) Li, H.; Wang, J.; Yang, L.; Song, Y. *Adv. Funct. Mater.* **2008**, *18*, 3258−3264.
(25) Wu, J.; Chen, J.; Qasim, K.; Xia, J.; Lei, W.; Wang, B.-p. *J. Chem. Technol. Biotechnol.* **2012**, *87*, 427−430.
(26) Zhang, J.; Huang, W.; Han, Y. *Macromol. Rapid Commun.* **2006**, *27*, 804−808.
(27) Wang, S.; Li, M.; Lu, Q. *ACS Appl. Mater. Interfaces* **2010**, *2*, 677−683.
(28) Xue, Z.; Wang, S.; Lin, L.; Chen, L.; Liu, M.; Feng, L.; Jiang, L. *Adv. Mater.* **2011**, *23*, 4270−4273.
(29) Zhu, Q.; Pan, Q.; Liu, F. *J. Phys. Chem. C* **2011**, *115*, 17464−17470.
(30) Zhang, J.; Seeger, S. *Adv. Funct. Mater.* **2011**, *21*, 4699−4704.
(31) Lim, H. S.; Baek, J. H.; Park, K.; Shin, H. S.; Kim, J.; Cho, J. H. *Adv. Mater.* **2010**, *22*, 2138−2141.
(32) Burger, C.; Hsiao, B. S.; Chu, B. *Annu. Rev. Mater. Res.* **2006**, *36*, 333−368.
(33) Zheng, J.; He, A.; Li, J.; Xu, J.; Han, C. C. *Polymer* **2006**, *47*, 7095−7102.
(34) Shang, Y.; Si, Y.; Raza, A.; Yang, L.; Mao, X.; Ding, B.; Yu, J. *Nanoscale* **2012**, *4*, 7847−7854.
(35) Viswanadam, G.; Chase, G. G. *Sep. Purif. Technol.* **2013**, *104*, 81−88.
(36) Yao, X.; Song, Y.; Jiang, L. *Adv. Mater.* **2011**, *23*, 719−734.
(37) Lim, T.-T.; Huang, X. *Ind. Crops Prod.* **2007**, *26*, 125−134.
(38) Lee, M. W.; An, S.; Joshi, B.; Latthe, S. S.; Yoon, S. S. *ACS Appl. Mater. Interfaces* **2013**, *5*, 1232−1239.
(39) Lin, J.; Ding, B.; Yu, J.; Hsieh, Y. *ACS Appl. Mater. Interfaces* **2004**, *2*, 521−528.
(40) Wang, J.; Raza, A.; Si, Y.; Cui, L.; Ge, J.; Ding, B.; Yu, J. *Nanoscale* **2012**, *4*, 7549−7556.
(41) Cassie, A.; Baxter, S. *Trans. Faraday Soc.* **1944**, *40*, 546−551.
(42) Tu, C.-W.; Tsai, C.-H.; Wang, C.-F.; Kuo, S.-W.; Chang, F.-C. *Macromol. Rapid Commun.* **2007**, *28*, 2262−2266.
(43) Boinovich, L. B.; Emelyanenko, A. M.; Pashinin, A. S.; Lee, C. H.; Drelich, J.; Yap, Y. K. *Langmuir* **2011**, *28*, 1206−1216.
(44) Panton, R. L. *Incompressible flow*, 3rd ed.; Wiley: New York, 2005.
(45) *KDS Legato 100 Manual*; KDScientific: Holliston, MA.
(46) Lin, J.; Ding, B.; Yang, J.; Yu, J.; Sun, G. *Nanoscale* **2012**, *4*, 176−182.
(47) Wu, J.; Wang, N.; Wang, L.; Dong, H.; Zhao, Y.; Jiang, L. *ACS Appl. Mater. Interfaces* **2012**, *4*, 3207−3212.
(48) Lin, J.; Shang, Y.; Ding, B.; Yang, J.; Yu, J.; Deyab, S. S. A. *Mar. Pollut. Bull.* **2012**, *64*, 347−352.
(49) Bradrup, J.; Immergut, E. H.; Grulke, E. A., Eds.; *Polymer Handbook*, 2nd ed.; Wiley: New York, 1975.